PREPRINT UCRL-80539

CONF-780314--4

Lawrence Livermore Laboratory

A TWO-DIMENSIONAL COMPUTER SIMULATION OF HYPERVELOCITY IMPACT CRATERING: SOME PRELIMINARY RESULTS FOR METEOR CRATER, ARIZONA

J. B. Bryan, D. E. Burton, M. E. Cunningham, and L. A. Lettis, Jr.

April 1978

This paper was prepared for submission to the Ninth Lunar and Planetary Science Conference, Houston, TX, March 13-17, 1978

This is a preprint of a paper intended for publication in a journal or proceedings. Since changes may be made before publication, this preprint is made available with the understanding that it will not be cited or reproduced without the permission of the author.

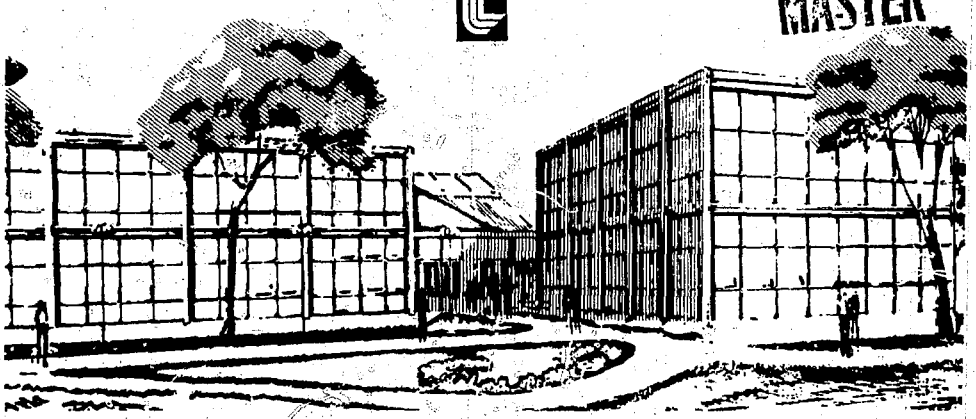

DISTRIBUTION OF THIS DOCUMENT IS UNLIMITED

A TWO-DIMENSIONAL COMPUTER SIMULATION OF HYPERVELOCITY IMPACT CRATERING: SOME PRELIMINARY RESULTS FOR METEOR CRATER, ARIZONA

J. B. Bryan, D. E. Burton, M. E. Cunningham, and L. A. Lettis, Jr.*

Earth Sciences Division
Lawrence Livermore Laboratory
Livermore, CA 94550

ABSTRACT

A computational approach used for subsurface explosion cratering has been extended to hypervelocity impact cratering. Meteor (Barringer) Crater, Arizona, was selected for our first computer simulation because it was the most thoroughly studied. It is also an excellent example of a simple, bowl-shaped crater and is one of the youngest terrestrial impact craters. Shoemaker estimates that the impact occurred about 20,000 to 30,000 years ago [Roddy (1977)]. Initial conditions for this calculation included a meteorite impact velocity of 15 km/s. meteorite mass of 1.57E+08 kg, with a corresponding kinetic energy of 1.88E+16 J (4.5 megatons). A two-dimensional Eulerian finite difference code called SOIL was used for this simulation of a cylindrical iron projectile impacting at normal incidence into a limestone target. For this initial calculation a Tillotson equation-of-state description for iron and limestone was used with no shear strength. A color movie based on this calculation was produced using computer-generated graphics. Results obtained for this preliminary calculation of the formation of Meteor Crater Arizona, are in good agreement with Meteor Crater measurements.

NOTICE
This report was prepared as an account of work sponsored by the United States Government. Neither the United States nor the United States Department of Energy, nor any of their employees, nor any of their contractors, subcontractors, or their employees, makes any warranty, express or implied, or assumes any legal liability or responsibility for the accuracy, completeness or usefulness of any information, apparatus, product or process disclosed, or represents that its use would not infringe privately owned rights.

* "Work performed under the auspices of the U.S. Department of Energy by the Lawrence Livermore Laboratory under contract number W-7405-ENG-48."

DISTRIBUTION OF THIS DOCUMENT IS UNLIMITED

INTRODUCTION

A computational technique used successfully for subsurface explosion cratering [Glenn and Thomsen (1976), Burton, et. al. (1975), Bryan, et. al. (1974), and Terhune, et. al. (1970)] has been extended to meteorite impact cratering. Meteor (Barringer) Crater, located between Winslow and Flagstaff, Arizona, was selected for this computer simulation. According to Nininger (1961), it has also been known as the Canyon Diablo Crater, Arizona Meteorite Crater, Coon Butte, and Crater Mound. The early-time or dynamic phase of the meteorite impact was treated with a two-dimensional Eulerian finite difference code called SOIL, written by Johnson (1977). The SOIL code was a derivative of the earlier DORF and RADOIL codes [Johnson (1970 and 1971)]. This treatment was similar that used in a pioneering effort by Bjork (1961), but it was extended to a time of 0.5 seconds or about an order of magnitude later in time. Recently O'keefe and Ahrens (1976, 1977) have reported calculations similar to that by Bjork but they placed their emphasis on ejecta dynamics. The late time or ballistic phase extrapolation was used to compute the final crater profile after the velocity field has been established in the mound region. This was done by computing an ejecta distribution based on ballistic trajectories followed by a slope stability adjustment. Parameters for the ballistic phase such as bulking factor and slope stability angle were selected from earlier explosion cratering studies [Bryan, et. al. (1974)].

This computational study of impact cratering was motivated by recent cratering meetings held at the U.S. Geological Survey in Flagstaff, Arizona. The symposium on Planetary Cratering Mechanics [see Roddy, et. al. (1977)] was held in 1976 followed by the Impact and Explosion Cratering Workshop held

in 1977. Earlier, impact and explosion cratering were topics at the Geophysical Laboratory - Lawrence Radiation Laboratory Cratering Symposium held at the Geophysical Laboratory of the Carnegie Institution in Washington, D. C., in 1961 [see Nordyke, Editor (1961)].

Meteorite Impact Conditions

Table I and Figure 1 show some estimated values for the Barringer meteorite impact velocity, mass, and kinetic energy which formed Meteor Crater, Arizona. Heide (1957) reports a range of 15 to 45 km/s for meteorite velocities. Estimates of meteorite impact velocity were bounded by Bjork (1961) between about 11 and 72 km/s. The escape velocity from the earth is about 11 km/s while the largest velocity any member of the solar system can have with respect to the earth is about 72 km/s. Shoemaker (1977) reports earth-crossing asteroids with velocities with respect to earth ranging between about 15 and 40 km/s. At least some of the meteorites have asteroidal origin [Wood (1968)]. The minimum impact velocity required to completely vaporize a meteorite has been estimated to be about 14 km/s [Zel'dovich and Raizer (1967)]. Apparently, most of the meteorite was vaporized in the formation of Meteor Crater, Arizona. Thus, the impact velocity for the Barringer meteorite is probably bounded between 11 and 40 km/s.

Estimates of Barringer meteorite mass vary over more than two orders of magnitude. Samplings of tiny spherical iron droplets in the area of Meteor Crater by Rinehart and Nininger led them to suggest that the mass of the meteorite was at least 1E+07 kg or greater [Baldwin (1963)]. In 1929 Moulton estimated the impact conditions as shown by the box in Figure 1. He arrived

at impact velocities between 11 and 24 km/s and mass between 4.6E+7 to 2.8E+9 by considering the work required to shear rock at the crater walls, crush and pulversize the rock within the crater, and heat the meteorite and adjacent rock mass. Other estimates made since 1929 have tended to be within the range of Moulton (see Figure 1). Nininger (1961) points out that the meteorite fragments found around the area of Meteor Crater have different chemical compositions suggesting that at least five different masses were involved. However, he indicates that a large single mass was probably responsible for excavating most of Meteor Crater since 90 to 95 percent of the fragments appear to have come from a single source [Nininger (1953)]. In general, the estimates of meteorite mass have larger uncertainties than corresponding estimates of impact velocity.

Bjork (1961) reported his calculation for Meteor Crater using an impact velocity of 30 km/s and a mass of 1.1E+7 kg (1.1 megatons). This calculation by Bjork is represented by the point marked (L) in Figure 1. Bjork ran the calculation to about a time of 0.06 s with a target material represented by tuff. After analyzing this calculation, Bjork estimated the actual impact conditions to be on a line of constant momentum labeled (k) in Figure 1. Lines of constant kinetic energy are also shown in Figure 1 for values of 1, 10, and 100 megatons. Shoemaker (1960, 1974) estimated values of near 1.7 megatons (I) and recently raised the estimate to about 4.5 megatons (F) [Roddy, et. al. (1975)]. Boddy, et. al. (1975) and Dence, et. al. (1977) have made estimates of 4.3 and 4.8 megatons, respectively [see Table I]. These are close to values selected for the initial impact conditions in our calculation which are similar to those by Shoemaker (1974). For our calculation

the meteorite mass, impact velocity, and corresponding kinetic energy were assumed to be 1.67E+8 kg, 15 km/s, and 1.88E+16 J (4.5 megatons), respectively. Thus, the impact kinetic energy for Meteor Crater was comparable to an estimate for the energy expended during the great volcanic eruption (on the order of 1E+16 J) which destroyed Krakatoa in 1883 [Short (1975)].

Some Calculational Assumptions

Bjork (1961) discussed many of the assumptions made for this type of computer calculation. The meteorite was treated as a right circular cylinder with length and diameter of 30 m impacting at normal incidence to the horizontal ground surface represented by a semi-infinite half-space. These assumptions introduce a vertical axis of rotational symmetry which permitted a two-dimensional rather than a three-dimensional simulation of the impact event. Bjork explains that based on hypervelocity experiments, impact crater shape and size are not strongly dependent on projectile shape provided that the aspect ratio (length divided by diameter) is about unity. Thus, this cylindrical projectile shape should be a reasonable approximation of the meteorite shape.

Materials in the calculation were described using the Tillotson equation-of-state description [Tillotson (1962)]. The nickel-iron meteorite, containing about 7 percent nickel and 90 percent iron [Nininger (1961)], was treated as iron of density 7,860 kg/m^3. The Moenkopi, Kaibab, Toroweap, Coconino, and Supai formations at the impact site were treated simply as a single limestone material of density 2,700 kg/m^3. Limestone was selected to approximate the impact site because the description was readily available [Allen (1967)] and

the Kaibab formation made up the major component of the ejecta. Roddy, et. al. (1975) describe the ejecta as about 65 percent Kaibab, 34 percent Coconino, and Toroweap, and 1 percent Moenkope. They reported that the Kaibab formation was about 80 to 95 m thick and consisted of sandy dolomite, dolomitic limestone, and minor calcareous sandstone. Earlier Nininger (1954) reported about 55 percent Kaibab, 13 percent Coconino, and 25 percent Moenkopi based on an excavation of rubble on the crater rim. The limestone density of 2,700 kg/m^3 is higher than the 2,300 kg/m^3 density reported by Regan and Hinze (1975). Bjork (1961) used tuff, a porous volcanic rock, with a density of 1,700 kg/m^3. Thus, the description of the meteorite is thought to be a better approximation than the description of the impact site.

In this initial calculation the materials had no shear strength. Bjork (1961) argues that the hypervelocity impact was essentially hydrodynamic in nature because the pressures involved greatly exceeded the strengths of the target materials. This assumption has been verified by our second SOIL calculation with material strengths included. Preliminary analysis of results show similar behavior. The crater radii were essentially unchanged while the crater depth, lip height, and crater volumes were reduced by about 8 percent in the calculation with elastic-plastic strength. No gravitational acceleration or overburden stresses were included in the dynamic phase of these simulations.

A portion of the computational mesh about the impact point is shown in Figure 2 at zero time when the meteorite (iron projectile) initially strikes the ground surface (limestone target) located at $z = -200$ m. The impact velocity was half the 30 km/s value used by Bjork (1961). The cylindrical

meteorite was 30 m in length and diameter compared with the value of 12 m used by Bjork. Thus, the meteorite mass was nearly sixteen times as large as the mass used by Bjork. The assumed initial impact velocity and mass are also shown. At this time the meteorite was represented by 32 zones 3.75 m on each side. This is relatively coarse zoning, at least when compared with the mass of the largest recovered meteorite fragment reported by Nininger (1961) - smallest zone mass: 1.3E+6 kg vs largest fragment: 6.4E+2 kg. The 100 x 100 m portion of the mesh in Figure 2 shows the rectangular zoning which was constructed using geometrically graded zone sizes increasing in both the +R and -Z directions. The outer boundaries were at about 3,000 m away from the impact point. This was sufficiently far away so that non-physical boundary effects would not occur. The SOIL grid used during the entire simulation consisted of about 11,000 zones, a grid of medium size, with 123 zones along the Z-axis and 91 zones along the R-axis. The regions above the limestone were iron and void which extended to the boundary located at Z = 0 m. Some iron and limestone mass flowed off the grid at Z = 0 m at later times.

Some Calculational Results

A. Dynamic Phase

Figures 3a through 3d show the calculated meteorite impact at about 0.0, 0.5, 1.0, and 1.5 ms on a 100 x 100 m portion of the grid. The velocity vectors indicate the direction of the mass flow with the maximum length representing 10,000 cm/s. Velocities exceeding the maximum value are shown as vectors with only half of an arrow head. The CGS system of units was used in the figures generated with the TENPLT computer graphics code

[Burton and Snell (1974)]. Material boundaries are shown as line segments connected at right angles. The Eulerian SOIL code permits mixed material zones or for this calculation zones with both iron and limestone. Tracer particles, each shown as an asterisk in the figures, were used to help define material boundaries and mass displacements in this Eulerian calculation. Initially, they were placed just inside the meteorite boundaries and in the limestone along planes at Z = -200, -250, -300, -350, and -400 m. Both vaporized iron and limestone began to jet upward and radially outward from the impact point. Figures 3e through 3h show the same sequence at times of about 2, 3, 4, and 5 ms. Vaporized iron with a density less than 10 kg/m^3 is labeled as a separate material. At 2 ms (Fig. 3e), the back of the meteorite, originally 30 m in length, is at the original ground surface. The front of the meteorite has been slowed down and compressed so that the length is about 20 m. Between 2 and 3 ms, the average velocity of the front of the meteorite has slowed to about 8 km/s. At 3 ms (Fig. 3f), the meteorite has penetrated to a depth of about 30 m, the original length of the meteorite. In Figures 3g and 3h the meteorite is vaporizing and breaking apart. These computer-generated figures parallel thesequence of cratering phenomena discussed by Roddy (1978).

Figures 4a through 4d show a similar sequence with pressure contours on a 100 x 100 m portion of the grid at times of about 0, 1, 2, and 3 ms with peak pressures of about 0, 4,330, 2,630, and 1,770 kilobars, respectively. The peak pressure of about 4,330 kilobars was in good agreement with Shoemaker's value (1960) of 4,500 kilobars for an impact velocity of 15 km/s. The isobars represent pressure values of 0, 38, 130, and 500 kilobars, respectively. The

values of 38 and 130 kilobars were selected to denote regions where high pressure polymorphs of silica, coesite and stishovite, might have been formed [Kaula (1968)]. Coesite and stishovite have been identified at Meteor Crater and were formed by the shock wave in the Coconino sandstone originally located between the depths of about 90 and 320 m below the original ground surface [Shoemaker and Kieffer (1974)]. Figures 4e through 4h show the corresponding velocity fields and pressure contours at about 5, 10, 25, and 50 ms with peak pressures of about 1,150, 520, 150, and 60 kilobars, respectively. The shock wave began entering the Coconino sandstone located at 90 m depth at about 5 ms. The meteorite was lagging the shock front at this time and reached this depth at about 13 ms. Figures 4e and 4f show a 200 x 200 m portion of the grid while figures 4g and 4h show a 600 x 600 m portion of the grid. Figure 5 shows the peak pressure vs the depth below the impact region along the Z axis. The calculated peak pressure in the Coconino sandstone is about 600 kilobars. Based on this calculation, Stishovite might be formed to a maximum initial depth of about 175 m. Similarly, coesite might be formed to a maximum initial depth of about 320 m or the bottom of the coconino sandstone. In this discussion it was assumed that the differences in shock impedance and other material properties across the material boundaries were negligible.

The energy partitioning between the iron and limestone is shown in Figure 6 in terms of kinetic and internal energy for times between 1 and 100 ms. The values are expressed in percent of the total original energy. At 1 ms the iron meteorite has about 87 percent of its original total energy (about 79 percent kinetic energy and about 8 percent internal energy). At

3.5 ms this value has dropped to about 50 percent (about 38 percent kinetic energy and about 12 percent internal energy). At 10 ms, 83 percent of the total energy has been transferred into the limestone. At 100 ms, the limestone has about 36 percent of the original energy as kinetic energy and about 58 percent as internal energy. Some mass of the meteorite left the calculationsl grid at the upper boundary at Z = 0 m located 200 m above the ground surface. At late times in the calculation the entire mass of the meteorite was vaporized.

The penetration depth p of the meteorite is shown in Figure 7 as a function of time. In the calculation the front of the projectile continued to penetrate downward until a depth of about 270 m was reached at about 0.3 s. At this late time the iron was a gas with a density less than about 10 kg/m^3. Nininger (1951) mentions that undisturbed sediments were found by drilling to depths of about 300 to 370 m. Similar results are also shown for Bjork's calculation which assumed an impact velocity of 30 km/s into the tuff. Although our calculation used only limestone in the target material, it is interesting to note the time and energy of the meteorite when it reaches a penetration depth corresponding to the depth of the coconino sandstone (about 90 m). This occurs at a time of about 13 ms when the meteorite has transferred about 87 percent of its energy to the target material (see Figure 6). This is somewhat larger than the 30 to 50 percent values estimated by Nininger (1956).

Summer and Charters performed some high velocity impact experiments using metal spheres and targets [Baker, et. al. (1973)]. They obtained the empirical expression listed in Table III to fit their data. Using an average

shock speed for the limestone of 5 km/s in this formula, we obtain the value P = 290 m. This differs from our calculated value of about 270 m by about 7 percent. Using the sonic value of 3 km/s [Ackermann et. al. (1975)], we obtain a larger value, P = 410 m.

Figure 8 shows the cavity at 0.5 s represented as contours of constant density with values of 0.01, 0.02, 0.05, 0.10, ..., 10 0 g/cc on a 500 x 500 m portion of the grid. This can be used to estimate an effective depth-of-burst for the explosive formation of Meteor Crater. If the lower part of the cavity is fit to a hemisphere, the center lies about 85 m below the original ground surface. The meteorite boundary shown in Figure 9 at the same time also fits a hemisphere centered approximately at the 85 m depth. Thus, even though the apparent energy source was migrating downward from the surface during the early times of impact, it appears that one might be able to use an effective depth-of-burst of about 85 m to compare Meteor Crater with nuclear explosive craters. Baldwin (1963) reported various estimates for the effective center of energy for the formation of Meteor Crater. These were about 64, 80, and 120 to 150 m by Johnson, Baldwin, and Shoemaker, respectively.

The tracer particles in Figure 9 outline the cavity growth leading to the characteristic rim uplift. The overturning of this flap as if it were hinged apparently occurred as a result of the material momentum in the gravitational field. This presumably led to the observed inverted stratigraphy at the crater rim.

B. Ballistic Phase

The final crater profiles were calculated using a ballistic throwout treatment followed by slope stability adjustment after the dynamic phase of the calculation which simulated the impact and stress-wave propagation. The velocity field at 0.5 s is shown for a 1000 x 2000 m portion of the grid in Figure 10. Contour lines of constant speed (the scalar magnitude of material velocity) ranging from 1,000 to 100,000 cm/s are shown superimposed on velocity vectors. The main shock front has passed beyond this portion of the grid and at this time is located between 200,000 and 300,000 cm away from the original impact region. Figure 11 shows the ejecta distribution as a function of distance after the ballistic treatment in a constant gravitational field for earth where G = 980 cm/s^2. Each computation zone was tested to see if it has sufficient vertical velocity to reach a prescribed height; normally this is taken to be the original ground surface. If this test was satisfied the zone is considered to be part of the ejecta and its mass was added to the ejecta distribution at the appropriate range. If this test fails, the zone mass was left at that location and considered to be part of the non-ejecta. A line which outlines the bottom of the cavity and terminates at the original ground surface marks the boundary between the calculated ejecta and the non-ejecta. The second profile line above it in Figure 11 shows the ejecta distribution which peaks near 55,000 cm. The volume of the ejecta has been increased by 20 percent since a bulking factor of 1.2 was used.

Figure 12 shows the calculated final crater profile where a slope stability adjustment was applied and the lower part of thecrater fit to a hyperbola. The values of 1.2 for the bulking factor and 35 degrees for the slope stability

angle were those chosen in earlier explosion cratering simulations [Bryan et. al. (1974)]. Other values of these parameters may prove to be more realistic in future impact cratering studies. The demarcation line between the ejecta and non-ejecta is also shown in Figure 12. Figure 13 shows the final crater calculated using a bulking factor of 1.0 (no bulking). Table IV shows that this appears to be a better fit to the observed data. One might argue that during the intervening 20,000 to 30,000 years, the effects of any original bulking would be minimized today. Figure 14 shows the final crater ejecta depth with respect to the demarcation line as a function of range. The calculated maximum range is about 2,500,000 cm. The peak at R = 30,000 cm appears to be a spurious effect caused by the proximity of the grid boundary 20,000 cm from the ground surface. The input and calculated crater parameters are summarized in Figure 15. A similar treatment using lunar gravity G = 162 cm/s^2 is shown in Figure 16. The final crater profile is larger than the earth crater (see Figure 12). The ejecta depth vs range is shown for the lunar case in Figure 17 which may be compared with Figure 13.

A comparison of the calculated final crater profile (G = 980 cm/s^2) and the actual crater profile [Shoemaker (1961)] is shown in Figure 18. Table IV summarizes several crater dimensions from the actual event and the calculation. These calculational results are in good agreement with the Meteor Crater in spite of the simplifying assumptions. These results, using a meteorite mass of 1.88E+8 kg and impact velocity of 15 km/s appear to fit the evidence although other sets of impact condition may also be permitted by the evidence (see Figure 1). Future calculational studies are planned which will use a multilayered impact site and more appropriate material

descriptions for the Moenkopi, Kaibab, Toroweap, Coconino, and Supai formations. Such detailed simulations when compared with the available geological evidence should extend our understanding of impact crater formation.

Meteor Crater and Nuclear Explosion Craters

The Canyon Diablo Meteorite, named after the nearest post office, formed the Meteor Crater. The following scaling approach is similar to those of Shoemaker and Roddy et. al. (1975). Shoemaker (1960) observed that Teapot Ess reproduced nearly all of the major structural features of Meteor Crater. This approach differs slightly by considering the entire data base of twelve buried nuclear cratering events by the U.S. These events are listed in Table V [after Nordyke (1977)]. Figure 19 shows the scaled apparent crater radius SR_A vs the scaled depth-of-burst SDOB. Apparent crater radius and yield data for each nuclear cratering event was used to calculate a kinetic energy for the Canyon Diablo Meteorite (see the right-hand column of Table V). These values shown in Table V range from about 1.7 to 260 megatons. Since Buggy was a row cratering event consisting of five charges and Sulky was deeply buried producing a mound or retarc rather than a crater, they were deleted from further considerations. Figure 19 shows significantly smaller scaled apparent crater radii for the near surface events Jangle S and Johnnie Boy as well as the deep event Palanquin. These three events predict very high energy values for W_B in Table V, so they were also deleted. The average and standard deviation for W_B for the remaining seven events were 4.5 ± 1.8 megatons (40 percent). This interval includes the estimates of Shoemaker (1974), Roddy et. al. (1975), and Dence et. al. (1977) as listed in

Table I. The current apparent crater depth D_A for Meteor Crater is 150 m [Roddy et. al. (1975)]. However, Roddy (1978) estimates that originally D_A was at least 200 m. Scaling these values gave scaled apparent crater depths of at least 17 and 13, respectively. In Figure 20, SD_A = 17 corresponds to about SDOB = 7.1 or an effective depth-of-burst EDOB for Meteor Crater of about 84 m. This value is very close to the value of 85 m discussed earlier from the computer simulation. Thus, the impact meteor crater appears to fit into the population of subsurface nuclear explosion craters with an effective depth-of-burst of about 85 m and a kinetic energy of about 4.5 megatons. The nuclear explosion sites listed in Table V are generally dry rather than wet sites which was probably representative of the arid region at the Canyon Diablo impact site (at least down to a depth of about 150 m).

SUMMARY

A computational approach used to simulate subsurface explosion cratering has been extended to an impact cratering simulation of the formation of Meteor Crater, a simple, bowl-shaped crater. The calculated results for a meteorite impacting at 15 km/s with a mass of 1.67E+8 kg are in good agreement with the observed crater. Studies are planned which will incorporate a more realistic multilayered geologic description of the impact site at Meteor Crater. A computational fracture model developed for coal fracture and controlled blasting studies [Burton et. al. (1977), Butkovich et. al. (1977), and Bryan et. al. (1977)] will be used in an attempt to correlate with observed fracture regions. Future studies are also planned for modeling other planetary and lunar impact craters including the larger, more complex craters with central uplift and ring features.

Computational tools, such as those demonstrated here, have proved to be very useful in the design and analysis of subsurface explosion cratering. Often successful explosion cratering studies have combined well-instrumented experiments with companion theoretical analyses. In the future, it is anticipated that such computational tools will play an increasingly important role in analyses of impact cratering.

ACKNOWLEDGMENTS

We wish to express our appreciation to Robert N. Schock and David J. Roddy who helped arouse our curiosity in the area of impact cratering and have provided continuing encouragement and support. John A. Blunden produced the color movie used to highlight our calculation. This work was performed under the auspices of the U. S. Department of Energy under Contract No. W-7405-ENG-48.

REFERENCES

Ackermann, H. D., Godson, R. H., and Watkins, J. S. (1975), A Seismic Refraction Technique used for Subsurface Investigations at Meteor Crater, Arizona, J. Geophys. Res. 80, 765-775.

Allen, R. T. (1967), Equation of State of Rocks and Minerals, General Atomic, San Diego, CA, Report GAMD-7834.

Baker, W. E., Westine, P. S., and Dodge, F. T. (1973), Similarity Methods in Engineering Dynamics: Theory and Practice of Scale Modeling, Hayden Book Co., Inc., Rochelle Park, NJ, pp 396.

Baldwin, R. B. (1963), The Measure of the Moon, University of Chicago Press, Chicago, 448 pp.

Bjork, R., (1961), Analysis of the Formation of Meteor Crater, Arizona: A Preliminary Report, J. Geophys. Res. 66, 3379-3387.

Reference to a company or product names does not imply approval or recommendation of the product by the University of California or the U.S. Department of Energy to the exclusion of others that may be suitable.

NOTICE

"This report was prepared as an account of work sponsored by the United States Government. Neither the United States nor the United States Department of Energy, nor any of their employees, nor any of their contractors, subcontractors, or their employees, makes any warranty, express or implied, or assumes any legal liability or responsibility for the accuracy, completeness or usefulness of any information, apparatus, product or process disclosed, or represents that its use would not infringe privately-owned rights."

Bryan, J. B., Burton, D. E., and Denny, M. D. (1974), Numerical Studies of Cratering in Bearpaw Shale: Two-Dimensional Results, Lawrence Livermore Laboratory, Livermore, CA., Report UCRL-51859.

Bryan, J., Snell, C., Hausinkveld, M., Burton, D., Bruce, L., Lettis, L., and Butkovich, T. (1977), Controlled Blasting Calculations and Experiments, Energy and Mineral Resource Recovery, American Nuclear Society Topical Meeting, April 12-14, Golden, CO., U.S. Department of Energy, Report CONF-770440, 663-672.

Burton, D. E., and Snell, C. M., (1974), User's Guide to TENPLT (TENSOR Graphics Code), and EOSLIB and XMUPGENS (Auxiliary Data Codes), U.S. Army Engineer Waterways Experiment Station, Vicksburg, MS, Misc. Paper E-74-1.

Burton, D. E., Snell, C. M., and Bryan, J. B. (1975), Computer Design of High-Explosive Experiments to Simulate Subsurface Nuclear Detonations, Nucl. Tech. 26, 65-87.

Burton, D. E., Lettis, L. A., Bryan, J. B., Butkovich, T. R., and Bruce, A. L. (1977), Anisotropic Creation and Closure of Tension Induced Fractures, Energy and Mineral Resource Recovery, American Nuclear Society Topical Meeting, April 12-14, Golden, CO, U.S. Department of Energy, Report CONF-770440, 673-683.

Butkovich, T. R., Burton, D. E., and Bryan, J. B. (1977), Calculational Modeling of Explosive Fracture and Permeability Enhancement, Energy and Mineral Resource Recovery, American Nuclear Society Topical Meeting, April 12-14, Golden, CO, U.S. Department of Energy, Report CONF-770440, 654-662.

Cunningham, M. E. (1974), User's Manual for the OIL Codes, Lawrence Livermore Laboratory, Livermore, CA, Report UCID-16605.

Dence, M. R., Grieve, R. A. F., and Robertson, P. B. (1977), Terrestrial Impact Structures: Principal Characteristics and Energy Considerations. In Impact and Explosion Cratering (D. J. Roddy, R. O. Pepin, and R. B. Merrill, Eds.), Pergamon Press, New York, 247-275.

Glenn, H. D., and Thomsen, J. M. (1976), Computer Simulation of a High-Explosive Cratering Experiment in a Complex Multilayered Geology, Lawrence Livermore Laboratory, Livermore, CA, Report UCRL-78155.

Heide, F. (1957), Meteorites, Translated by E. Anders and E. Dufresne, The University of Chicago Press, Chicago, 144 pp.

Johnson, W. E. (1970), Development and Application of Computer Programs Related to Hypervelocity Impact, Systems, Science, and Software, LaJolla, CA, Report 3SR-353, ARPA Order No. 854.

Johnson, W. E. (1971), RADOIL and RAM, Systems, Science, and Software, La Jolla, CA, Report 3SR-104, DASA-2649.

Johnson, W. E. (1977), Prepublication Communication on the SOIL Code, Computer Code Consultants, Los Alamos, NM.

Kaula, W. M. (1968), An Introduction to Planetary Physics: The Terrestrial Planets, John Wiley and Sons, Inc., New York, 490 pp.

Nininger, H. H. (1951), A Resume of Researches at the Arizona Meteorite Crater, The Scientific Monthly, LXXII, No. 2, 75-86.

Nininger, H. H. (1953), A Comet Strikes the Earth, 4th Rev., Desert Press, Inc., Palm Desert, CA, 76pp.

Nininger, H. H. (1954), Impactite Slag at Barringer Crater, American Journal of Science, 252, 277-290.

Nininger, H. H. (1956), Arizona's Meteorite Crater: Past - Present - Future, American Meteorite Laboratory, Denver, CO, 232 pp.

Nininger, H. H. (1961), Ask a Question About Meteorites, American Meteorite Laboratory, Denver, CO, 87 pp.

Nordyke, M. D., - Editor (1961), Proceedings of the Geophysical Laboratory - Lawrence Radiation Laboratory, Livermore, CA, Report UCRL-6438, Parts I and II.

Nordyke, M. D. (1977), Nuclear Cratering Experiments: United States and Soviet Union, In Impact and Explosion Cratering (D. J. Roddy, R. O. Pepin, and R. B. Merrill, Eds.). Pergamon Press, New York.

O'Keefe, J. D., and Ahrens, T. J. (1976), Impact Ejecta on the Moon, Proc. Lunar Sci. Conf. 7th, p. 3007-3025.

O'Keefe, J. D., and Ahrens, T. J. (1977), Meteorite Impact Ejecta: Dependence of Mass and Energy Lost on Planetary Escape Velocity, Science 198, 1249-1251.

Regan, R. D., and Hinze, W. J. (1975), Gravity and Magnetic Investigations of Meteor Crater, Arizona, J. Geophys. Res. 80(5), 776-782.

Roddy, D. J., Peppin, R. O., and Merrill, R. P. - Editors (1977), Impact and Explosion Cratering - Planetary and Terrestrial Implications Pergamon Press, New York, 1301 pp.

Roddy, D. J., Boyce, J. M., Colton, G. W., and Dial, A. L., Jr. (1975), Meteor Crater, Arizona, Rim Drilling with Thickness, Structural Uplift, Diameter, Depth, Volume and Mass Balance Calculations, Proc. Lunar Sci. Conf. 6th, p. 2621-2644.

Roddy, D. J. (1977), Large-scale Impact and Explosion Craters: Comparisons of Morphological and Structural Analogs, In Impact and Explosion Cratering (D. J. Roddy, R. O. Peppin, and R. B. Merrill, Eds.), Pergamon Press, New York, 185-246.

Roddy, D. J. (1978), Cratering Motions for Bowl-Shaped Impact Craters: A Phenomenological Sequence of Events, Proc. Lunar Sci. Conf. 9th, This volume.

Shoemaker, E. N. (1960), Penetration Mechanics of High Velocity Meteorites, Illustrated by Meteor Crater, Arizona. In Structure of the Earth's Crust and Deformation of Rocks, p. 418-434. Intl. Geol. Cong., XXI Session, Pt. 18, Copenhagen.

Shoemaker, E. M. (1961), Geological Interpretation of Lunar Craters, U.S. Department of Interior Geological Survey, Administrative Report, 139 pp.

Shoemaker, E. M. (1963), Impact Mechanics at Meteor Crater, Arizona, in the Moon, Meteorites, and Comets (B. M. Middlehurst and G. P. Kuiper, Eds.), p 301-336, University of Chicago Press, Chicago.

Shoemaker, E. M., and Kieffer, S. W. (1974), Guidebook to the Geology of Meteor Crater, Arizona, Prepared for the 37th Annual Meeting of the Meteoritical Society.

Shoemaker, E. M. (1977), Astronomically Observable Crater-Forming Projectiles, In Impact and Explosion Cratering (D. J. Roddy, R. O. Peppin, and R. B. Merrill, Eds.), Pergamon Press, New York, 617-628.

Short, N. M. (1975), Planetary Geology, Prentice-Hall, Inc., Englewood Cliffs, NJ, 361 pp.

Sun, J. M. S. (1970), Energy Counter-Pressure Scaling Equations of Linear Crater Dimensions, J. Geophys. Res. 75, 2003-2027.

Terhune, R. W., Stubbs, T. F., and Cherry, J. T. (1970), Nuclear Cratering on a Digital Computer. In Proceedings, Symposium on Engineering with Nuclear Explosives, January 14-16, Las Vegas, NV, p 334-359, American Nuclear Society and U.S. Atomic Energy Commission, Report CONF-700101 (Vol. I).

Tillotson, J. H. (1962), Metallic Equations of State for Hypervelocity Impact, General Atomic, San Diego, CA, Report GA-3216, 139 pp.

Vdovykin, G. P. (1973), The Canyon Diablo Meteorite, Space Sci. Rev., 14, 758-772.

Vortman, L. J. (1970), Nuclear Excavation. In Education for Peaceful Uses of Nuclear Explosives (Editor: L. E. Weaver), p 65-79. The University of Arizona Press, Tuscon, AZ.

Wood, J. A., (1968), Meteorites and the Origin of Planets, McGraw-Hill Book Co., New York, 117 pp.

Zel'dovich, Ya. B., and Raizer, Yu. R. (1967), Physics of Shock Waves and High-Temperature Hydrodynamic Phenomena (W. D. Hayes and R. F. Probstein, Eds.) Vol. 2, 845 pp, English Translation, Academic Press, New York.

TABLE I. A list of some estimates of impact mass, velocity, and kinetic energy for the Barringer Meteorite.

Source	Mass (kg)	Velocity (km/s)	Kinetic Energy (J)	Kinetic Energy (megatons)	Reference
Rinehart (1958)	$>1.1\times10^{7}$	--	--	--	Bjork (1961)
Baldwin (1949)	--	--	3.0×10^{14}	0.07	Dence, et. al. (1977)
Bjork (1961) calculation	1.1×10^{7}	30	4.8×10^{15}	1.1	Bjork (1961)
Shoemaker (1960)	6.3×10^{7}	15	7.1×10^{15}	1.7	Shoemaker (1977)
Beals & Innes (1964)	4.7×10^{7}	20	9.4×10^{15}	2.4	Vdovykin (1977)
Sun (1970)	1.4×10^{8}	15	1.5×10^{16}	3.7	Sun (1970)
Roddy et. al. (1975)	--	--	1.8×10^{16}	4.3	Roddy et. al. (1975)
Shoemaker (1974)	1.7×10^{8}(a)	15	1.9×10^{16}	4.5	Roddy et. al. (1975)
Dence et. al. (1977)	--	--	2.0×10^{16}	4.8	Dence et. al. (1977)
Kopal (1966)	2.7×10^{8}(a)	15	3.1×10^{16}	7.3	Vdovykin (1977)
Baldwin (1963)	2.6×10^{8}	16	3.4×10^{16}	8.1	Baldwin (1963)
Cook (1964)	1.4×10^{8}	30	6.5×10^{16}	16	Vdovykin (1977)
Opik (1961)	2.2×10^{9}	16	2.8×10^{17}	67	Opik (1961)
Opik (1958)	2.6×10^{9}	15	2.9×10^{17}	70	Opik (1961)
OUR INITIAL CALCULATION	1.7×10^{8}	15	1.9×10^{16}	4.5	

(a) The published mass value was changed to make it consistent with corresponding velocity and kinetic energy values.

TABLE II. Tillotson equation of state parameters for iron and limestone.

	Iron	Limestone
ρ_o (g/cm^3)	7.86	2.70
a (-)	0.50	0.50
E_o (ergs/g)	9.5×10^{10}	1.0×10^{11}
b (-)	1.50	0.60
A (ergs/3)	1.379×10^{12}	4.0×10^{11}
E_s (ergs/cm^3)	2.44×10^{10}	2.5×10^{10}
E_s' (ergs/g)	1.02×10^{11}	1.4×10^{11}
α (-)	5.0	5.0
β (-)	5.0	5.0
B (ergs/cm^3)	1.05×10^{12}	6.7×10^{11}

The Tillotson equations for the gaseous and solid regions are:

$$PGAS = \frac{aE}{V} + \left\{ \frac{b\frac{E}{V}}{\frac{E}{E_0\left(\frac{V_0}{V}\right)^2}+1} + A\mu e^{-\alpha\left(\frac{V}{V_0}-1\right)} \right\} e^{-\beta\left(\frac{V}{V_0}-1\right)^2}$$

$$PSOL = \frac{E}{V}\left\{ a + \frac{b}{\frac{E}{E_0\left(\frac{V_0}{V}\right)^2}+1} \right\} + A\mu + B\mu^2 .$$

V = specific volume = $\frac{1}{\rho}$

V_o = normal specific volume = $\frac{1}{\rho_o}$

$\mu = \frac{V_o - V}{V}$

E = specific internal energy (with radiation energy subtracted out)

$PGAS$ = pressure of gaseous material

$PSOL$ = pressure of solid material or of material whose specific internal energy is below the vaporization energy.

See Cunningham (1974), Allen (1967), and Tillotson (1962) for additional details.

TABLE III. Empirical penetration formula by Summers and Charters [after Baker et. al. (1973)].

$$P/d = 2.28 \left(\frac{\rho V}{\rho t \, C_t}\right)^{2/3}$$

d:	projectile diameter	30 m
ρ:	projectile density	7,860 kg/m^3
ρt:	target density	2,700 kg/m^3
V:	projectile impact velocity	15 km/s
C_t:	target sonic velocity	5 km/s*
P:	penetration depth	P = 290 m

*The value C_t = 5 km/s was chosen as an estimate of the average shock velocity during the first 0.5 s after impact.

TABLE IV. A comparison of calculated and actual crater dimensions for Meteor Crater, Arizona.

	ACTUAL	CALCULATED			
	Roddy, et. al. (1975)	Bulking Factor = 1.2 angle = 35°		Bulking Factor = 1.0 angle = 35°	
			Percent Difference		Percent Difference
Apparent Crater Radius (m)	518	485	-6%	505	-3%
Apparent Crater Depth (m)	150*	194	+29%	194	+29%
Apparent Crater Volume (m^3)	7.60×10^7	6.35×10^7	=16%	6.99×10^7	-8%
Apparent Lip Crater Radius (m)	593	606	+2%	606	+2%
Apparent Lip Crater Height (m)	47.0**	78.0	+66%	66.9	+42%
Apparent Lip Crater Volume (m^3)	1.25×10^8	1.35×10^8	+8%	1.32×10^8	+6%

*Roddy (1978) estimates that the original crater depth was at least 200 m.

**Roddy et. al. (1975) indicate that the original cracer lip height has been reduced by erosion during the intervening 20,000 to 30,000 years.

TABLE V. An energy estimate for Barringer Crater Based on U.S. nuclear cratering data.

	Medium	Yield: W (kt)	Depth of Burst DOB (m)	Apparent Crater Depth D_A (m)	Apparent Crater Radius R_A (m)	Scaled Apparent Crater Parameters SDOB SD_A SR_A $m/(kt)^{1/3.4}$			Energy of Barringer Meteorite $W_B(Mt) = \left[\frac{(R_A)_B}{(R_A)_i}\right]^{3.4} \frac{W_i\ (kt)}{1000}$
1. Teapot ESS	Alluvium[a]	1.2	20	27	45	19	26	43	4.9
2. Danny Boy	Basalt[b]	0.42	34	19	33	44	25	43	4.9
3. Sedan	Alluvium[c]	100	194	98	184	50	25	47	3.4
4. Cabriolet	Rhyolite[b]	2.6	52	37	54	39	28	41	5.7
5. Schooner	Tuff[d]	35	108	63	130	38	22	46	3.9
6. Jangle U	Alluvium[a]	1.2	5.2	16	40	4.9	15	38	7.3
7. Neptune	Tuff[a]	0.115	31	11	31	49	21	59	1.7
8. Jangle S	Alluvium[a]	1.2	1.1	6.4	14	1.0	6	13	260
9. Johnnie Boy	Alluvium[a]	0.5	0.53	9.1	18	0.6	11	22	46
10. Palanquin	Rhyolite[b]	4.3	85	24	36	55	16	23	37
11. Sulky (retarc)	Basalt[b]	0.087	27	--	--	55	--	--	--
12. Buggy (row crater)	Basalt[b]	1.1x5	41	21	38	40	20	37	7.9-40

References: Nordyke (1977); Roddy, et. al. (1975); Vortman (1970), SAMPLE: 1-7 4.5 ± 1.8(Mt) (40%)

Water conditions:

a. Dry b. Dry (<1%) c. Dry (~20%) d. Wet (~10%) but unsaturated.

Figure Captions - incomplete list - others on figures

FIGURE 3 a - 3 h	Velocity field; speed contours
Figure 4 a - 4 h	Velocity field; pressure contours
Figure 8	Density contours
Figure 9	Density contours with tracer particles
Figure 10	Velocity field for ballistic throwout
Figure 11	Ejecta distribution
Figure 12	Final crater; 1.2 bulking factor
Figure 13	Final crater; 1.0 bulking factor
Figure 14	Ejecta depth versus range
Figure 15	Parameter Summary
Figure 16	Final lunar crater; 1.2 bulking factor
Figure 17	Lunar ejecta depth versus range

SOME ESTIMATED IMPACT CONDITIONS FOR METEOR CRATER, ARIZONA

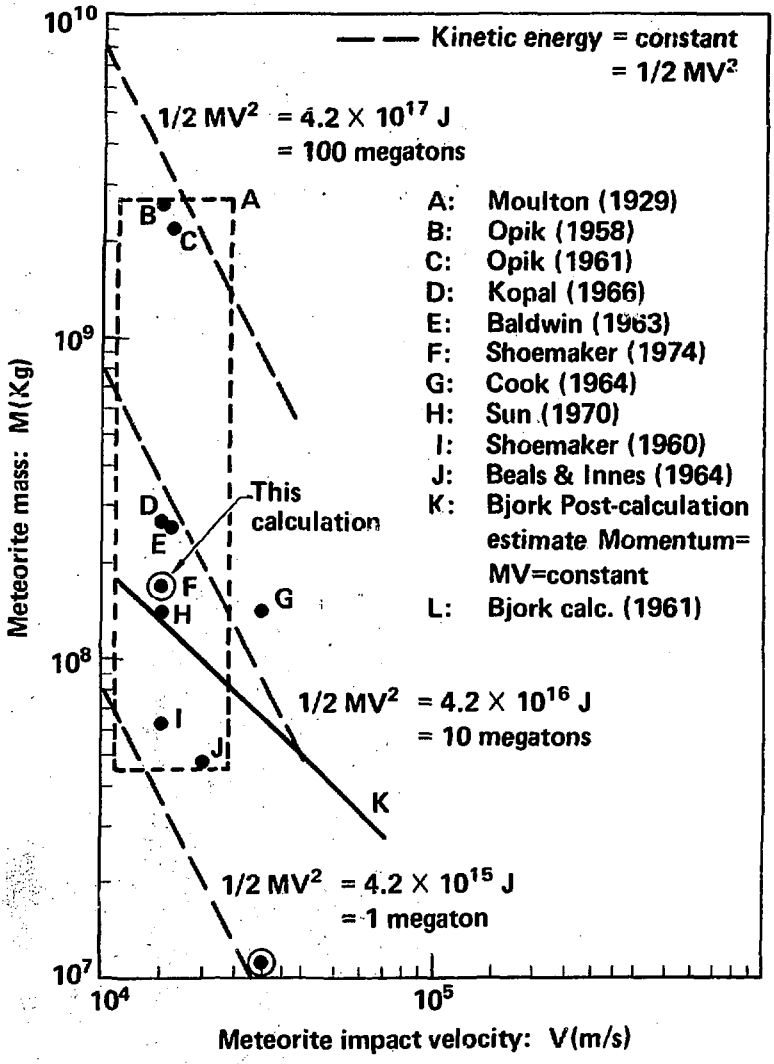

Bryan, J.B.
Crater. Sim.
Figure 1.

PORTION OF CALCULATIONAL MESH WITH MATERIALS

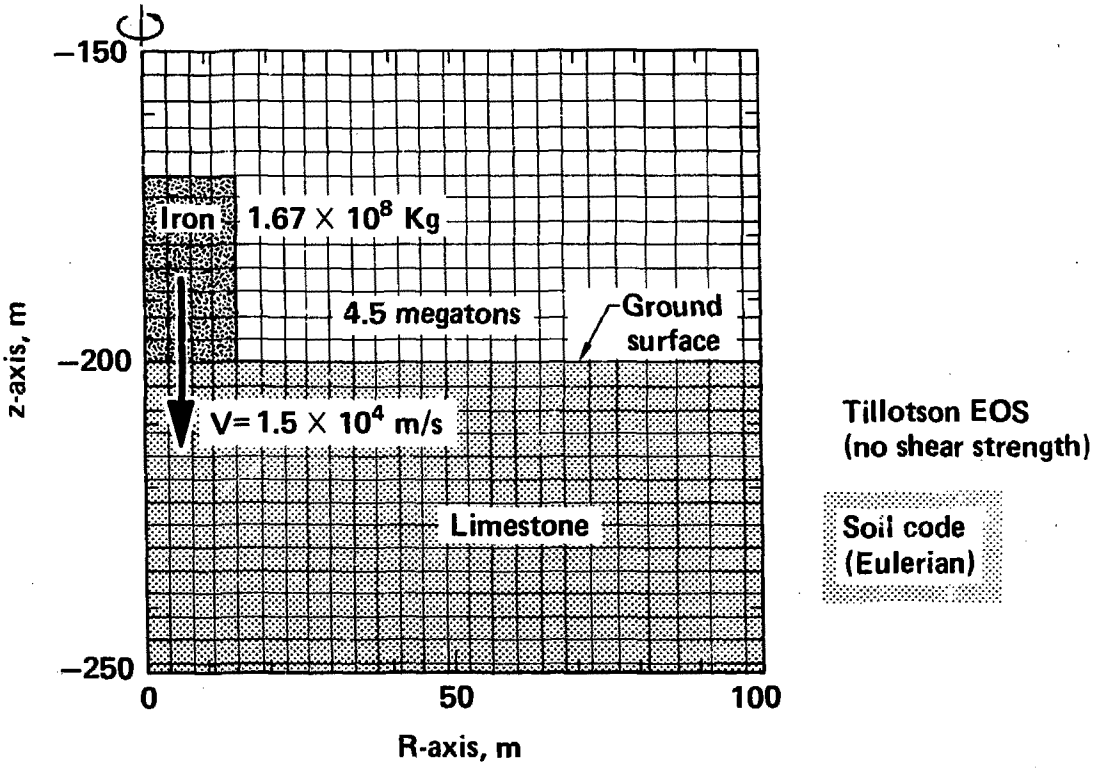

Bryan, J.B.
Crater. Sim.
Figure 2

20: VECTOR U V 0 1E4 RZ 30 M T

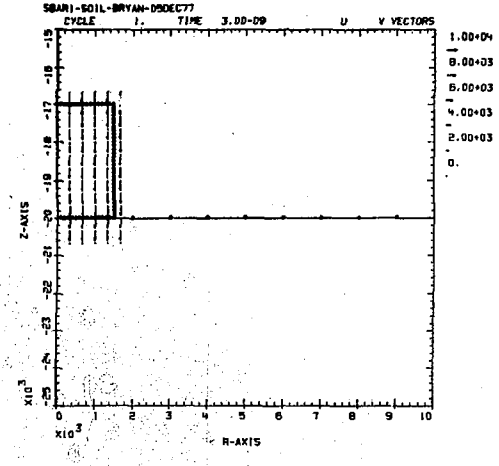

Bryan, J. B.
Crater. Sim.
Figure 3 a

20: VECTOR U V 0 1E4 RZ 3D M T

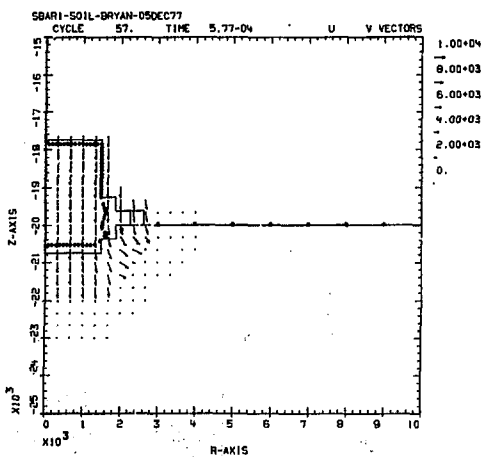

Bryan, J. B.
Crater Sim.
Figure 3 b

20: VECTOR U V C IEV RZ 30 M 1

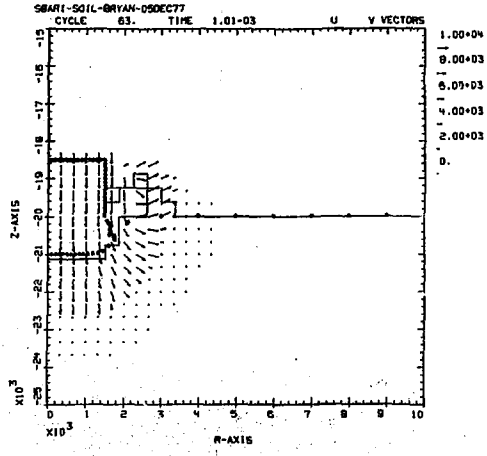

Bryan, J. B.
Crater Sim.
Figure 3 c

20: VECTOR U V 0 1E4 RZ 30 M T

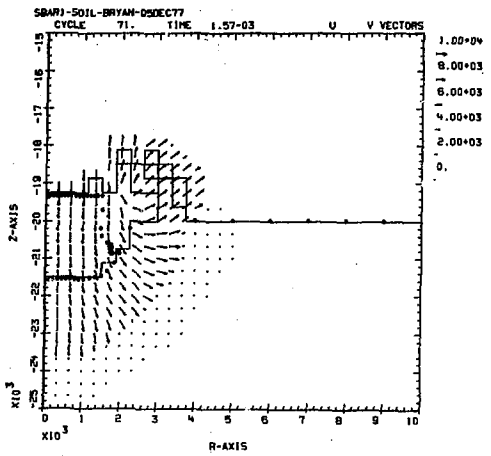

Bryan, J. B.
Crater Sim.
Figure 3 d

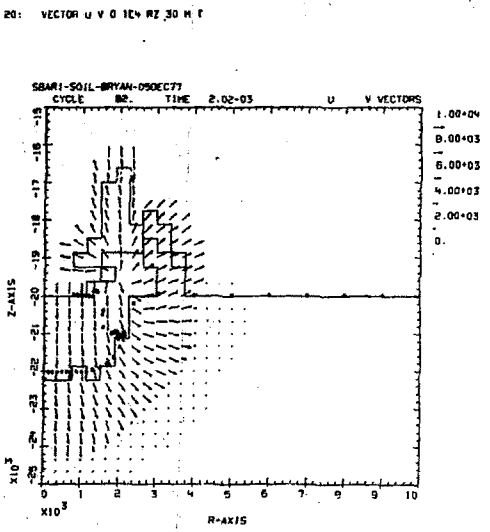

Bryan, J. B.
Crater. Sim.
Figure 3e

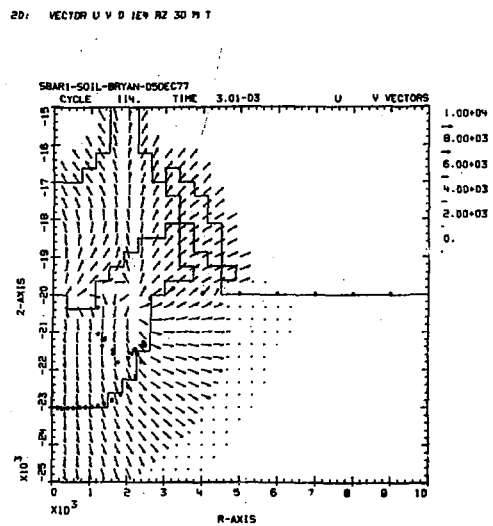

Bryan, J. B.
Crater. Sim.
Figure 3 f

20: VECTOR U V D IE4 RZ 30 M T

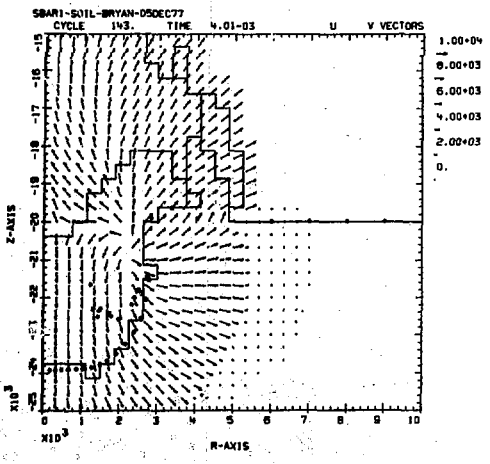

Bryan, J. B.
Crater. Sim.
Figure 3 g

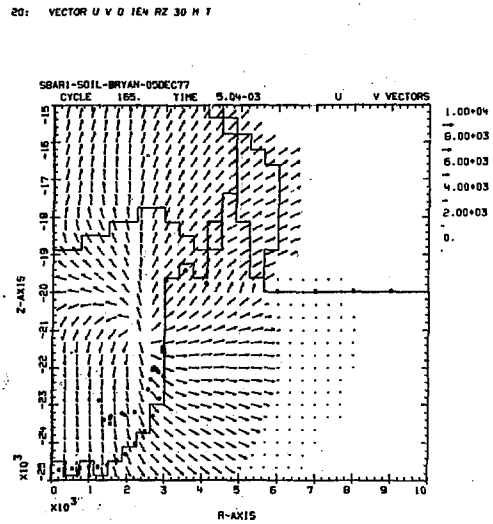

Bryan, J. B.
Crater. Sim.
Figure 3 h

B: OVERLAY VECTOR U V 0 1E4 RZ 30 CON P 0 30E9 130E9 500E9 L M

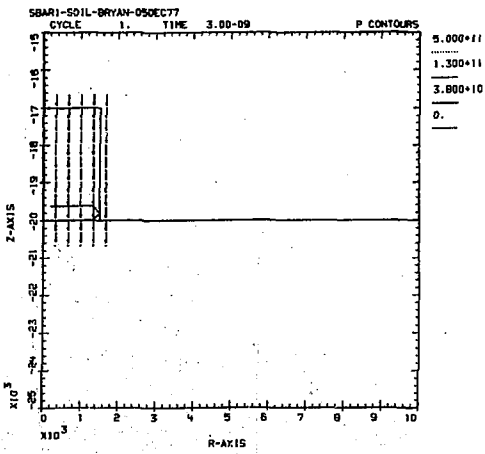

Bryan, J. B
Crater. Sim.
Figure 4 a

8: OVERLAY VECTOR U V 0 1E4 RZ 3D CON P 0 30E9 130E9 500E9 L H

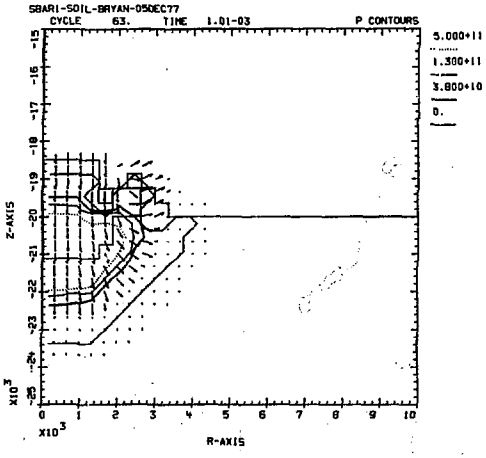

Bryan, J. B.
Crater Sim.
Figure 4-6

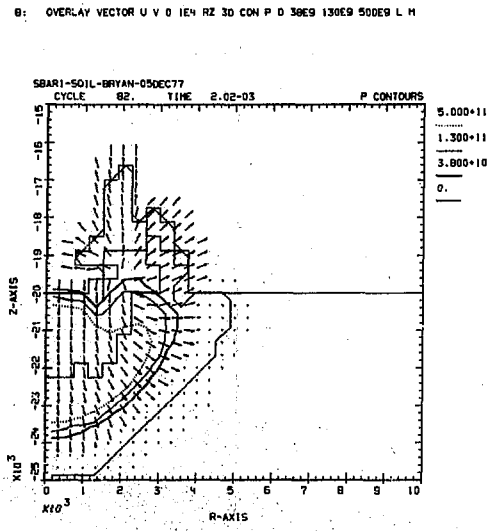

Bryan, J. B.
Crater. Sim.
Figure 4 c

B: OVERLAY VECTOR U V 0 1E4 RZ 3D CON P 0 38E9 130E9 500E9 L M

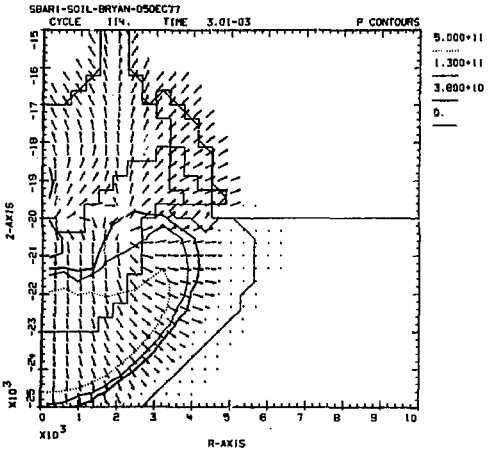

Bryan, J. B.
Crater. Sim.
Figure 4 d

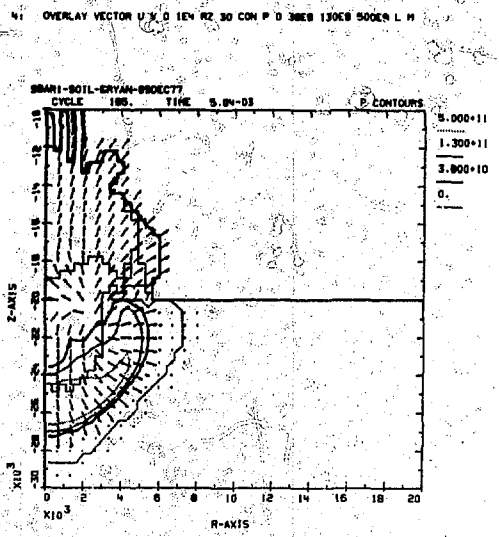

Bryan, J. B.
Crater. Sim.
Figure 4 e

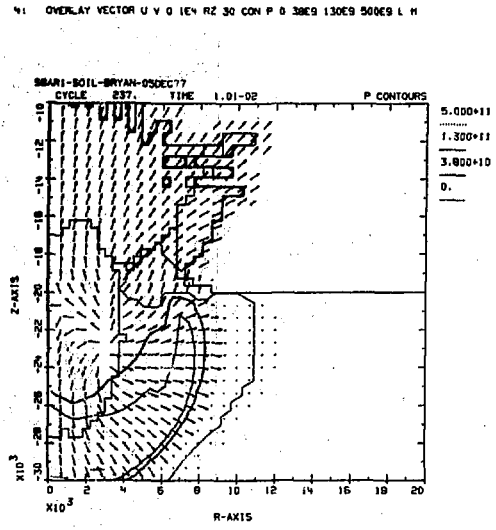

Bryan, J. B.
Crater, Sim.
Figure 4 f

12: OVERLAY VECTOR U V 0 1E4 RZ 30 CON P 0 30E9 130E9 500E9 L H

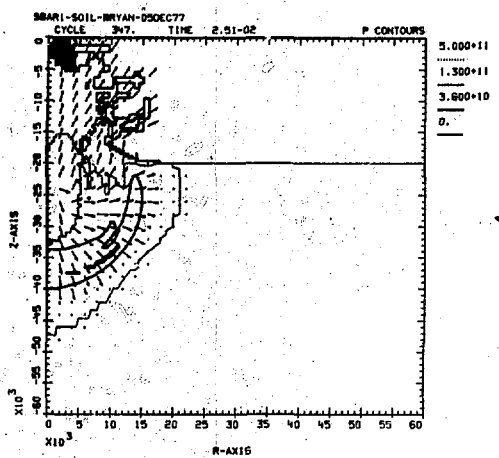

Bryan, J. B.
Crater. Sim.
Figure 4 g

12: OVERLAY VECTOR U V 0 1E4 RZ 30 CON P 0 30E9 130E9 500E9 L 11

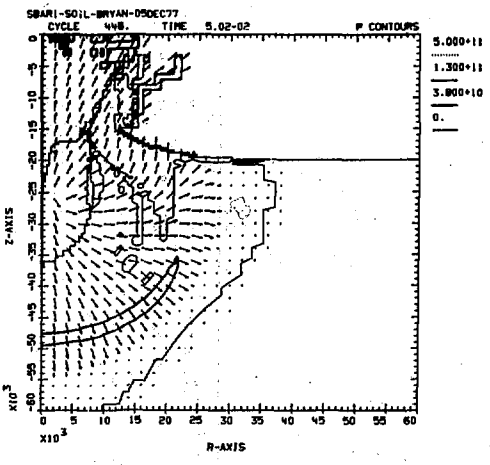

Bryan, J. B.
Crater. Sim.
Figure 4 h

CALCULATED PEAK PRESSURE VS. DEPTH BELOW IMPACT REGION

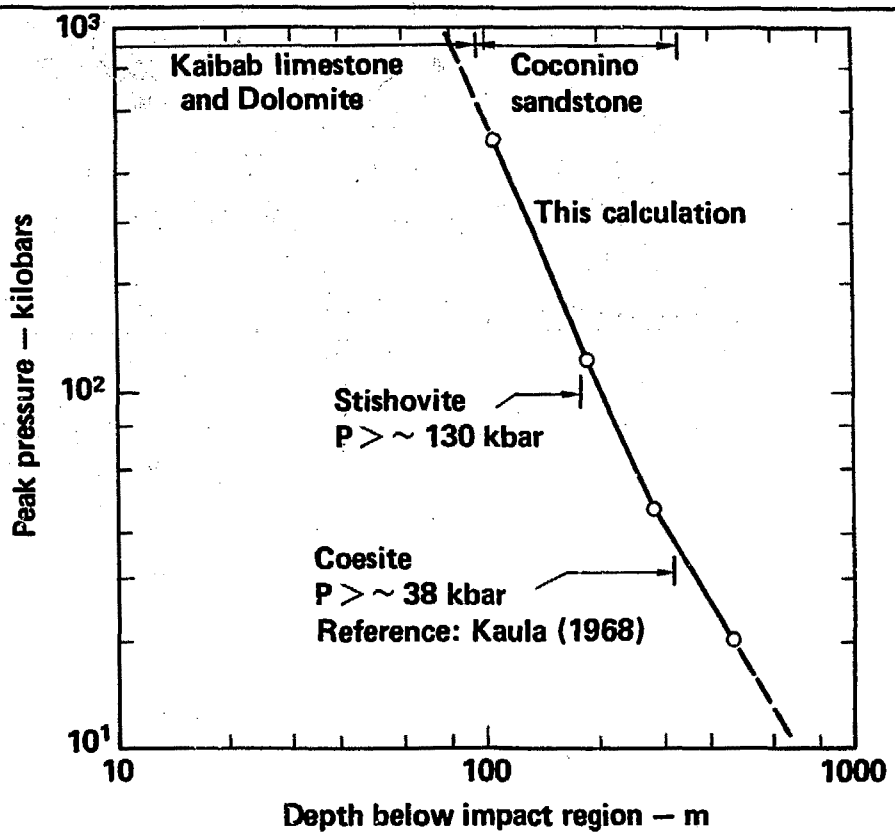

Bryan, J. B.
Crater. Sim.
Figure 5

ENERGY PARTITIONING VERSUS TIME

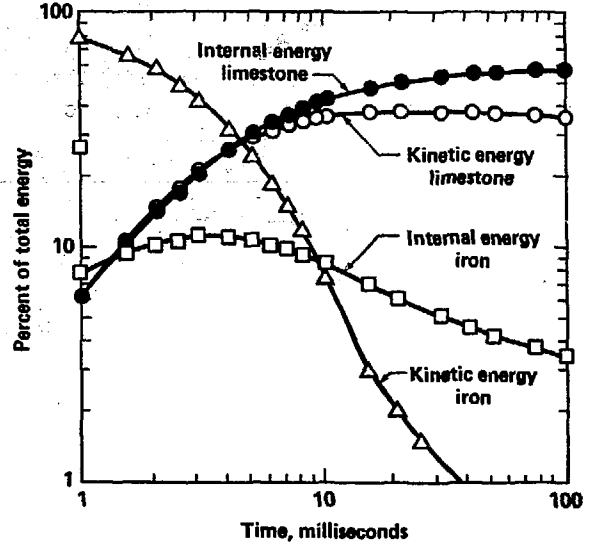

Bryan, J. B.
Crater. Sim.
Figure 6

METEORITE PENETRATION DEPTH VERSUS TIME

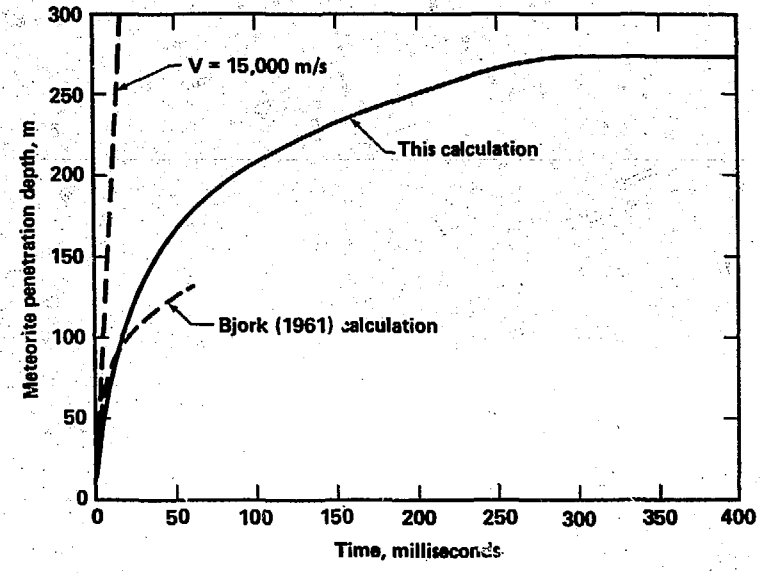

Bryan, J. B.
Crater. Sim.
Figure 7

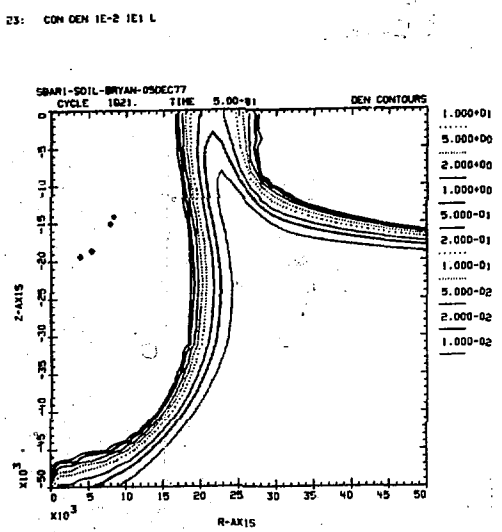

Bryan, J. B.
Crater. Sim.
Figure 8

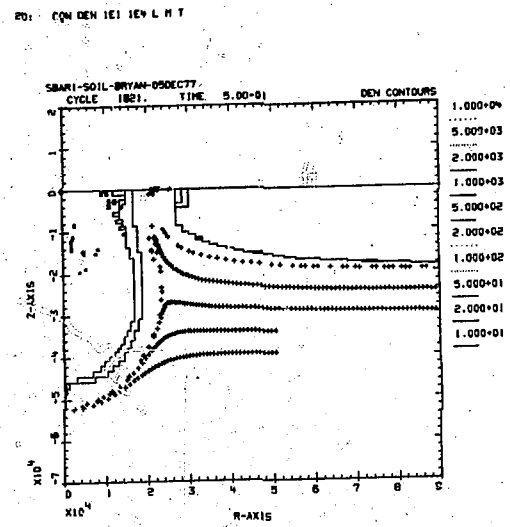

Bryan, J. B.
Crater. Sim.
Figure 9

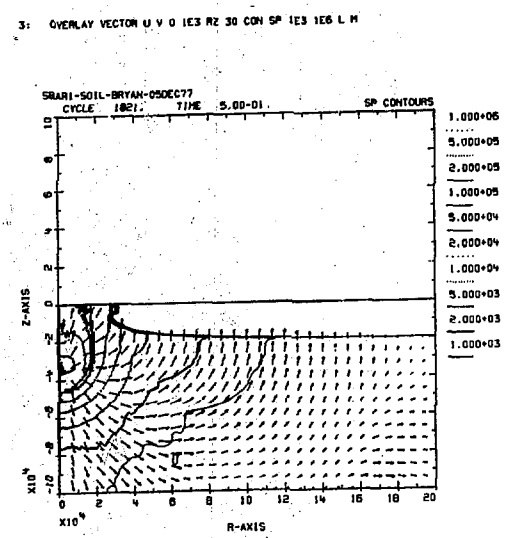

Bryan, J. B.
Crater. Sim.
Figure 10

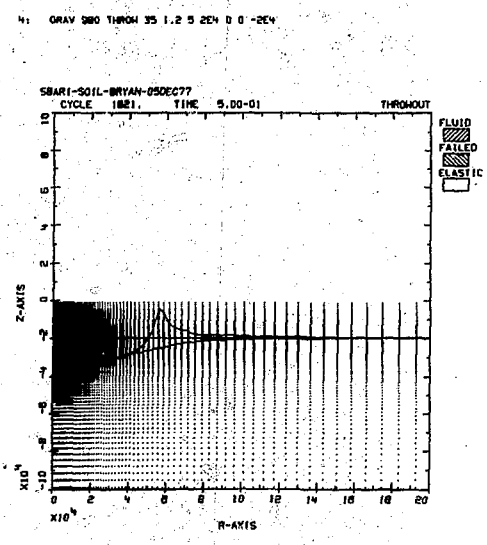

Bryan, J. B.
Crater. Sim.
Figure 11

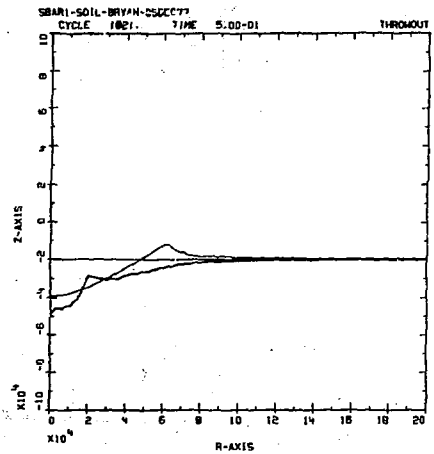

Bryan, J. B.
Crater. Sim.
Figure 12

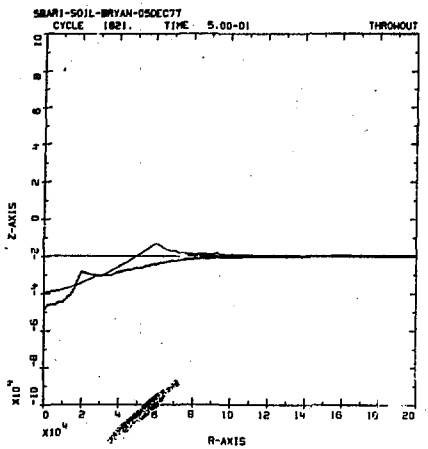

Bryan, J. B.
Crater. Sim.
Figure 13

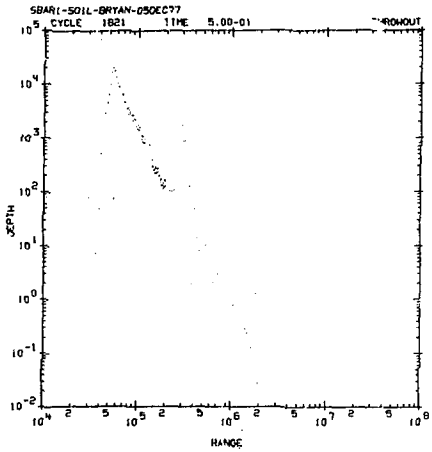

Bryan, J. E.
Crater. Sim.
Figure 14

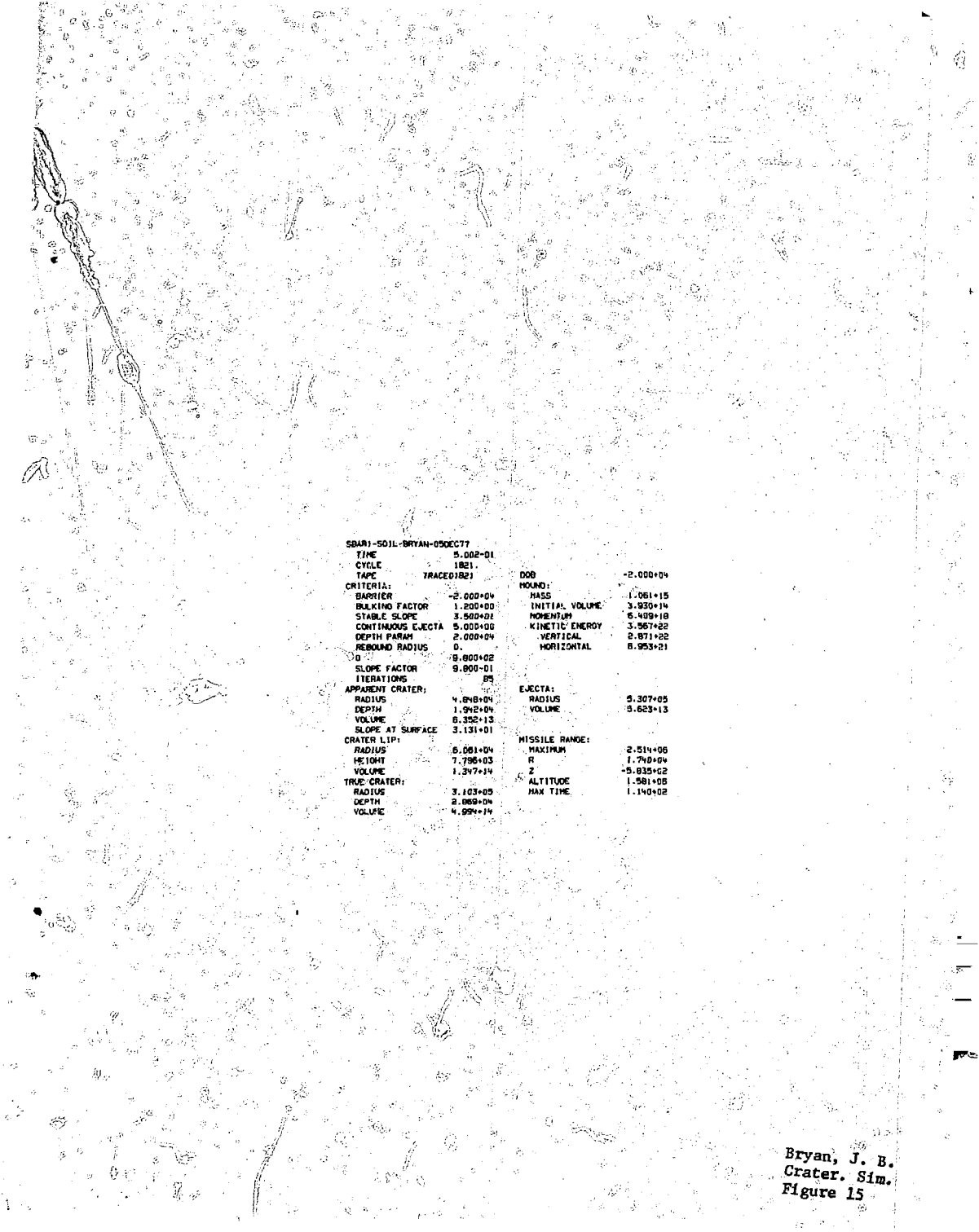

SBAR)-SOIL-BRYAN-050EC77

TIME	5.002-01		
CYCLE	1821.		
TAPE	TRACED182)	DOB	-2.000+04
CRITERIA:		MOUND:	
BARRIER	-2.000+04	MASS	1.061+15
BULKING FACTOR	1.200+00	INITIAL VOLUME	3.930+14
STABLE SLOPE	3.500+01	MOMENTUM	6.409+18
CONTINUOUS EJECTA	5.000+00	KINETIC ENERGY	3.567+22
DEPTH PARAM	2.000+04	VERTICAL	2.871+22
REBOUND RADIUS	0.	HORIZONTAL	8.953+21
D	9.800+02		
SLOPE FACTOR	9.800-01		
ITERATIONS	85		
APPARENT CRATER;		EJECTA:	
RADIUS	4.848+04	RADIUS	5.307+05
DEPTH	1.942+04	VOLUME	5.623+13
VOLUME	6.352+13		
SLOPE AT SURFACE	3.131+01		
CRATER LIP:		MISSILE RANGE:	
RADIUS	6.061+04	MAXIMUM	2.514+06
HEIGHT	7.796+03	R	1.740+04
VOLUME	1.347+14	Z	-5.835+02
TRUE CRATER:		ALTITUDE	1.581+06
RADIUS	3.103+05	MAX TIME	1.140+02
DEPTH	2.869+04		
VOLUME	4.994+14		

Bryan, J. B.
Crater. Sim.
Figure 15

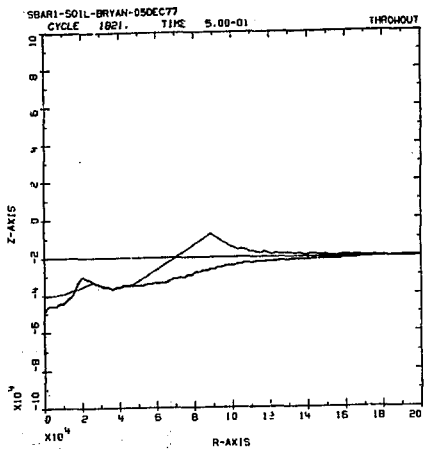

Bryan, J. B.
Crater. Sim.
Figure 16

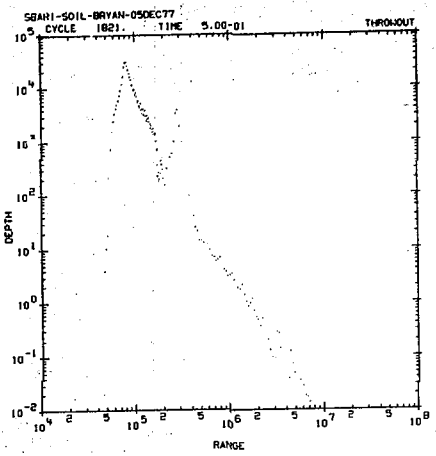

Bryan, J. B.
Crater. Sim.
Figure 17

CROSS SECTION, OF METEOR CRATER, ARIZONA

(Drawn after Shoemaker, 1960)

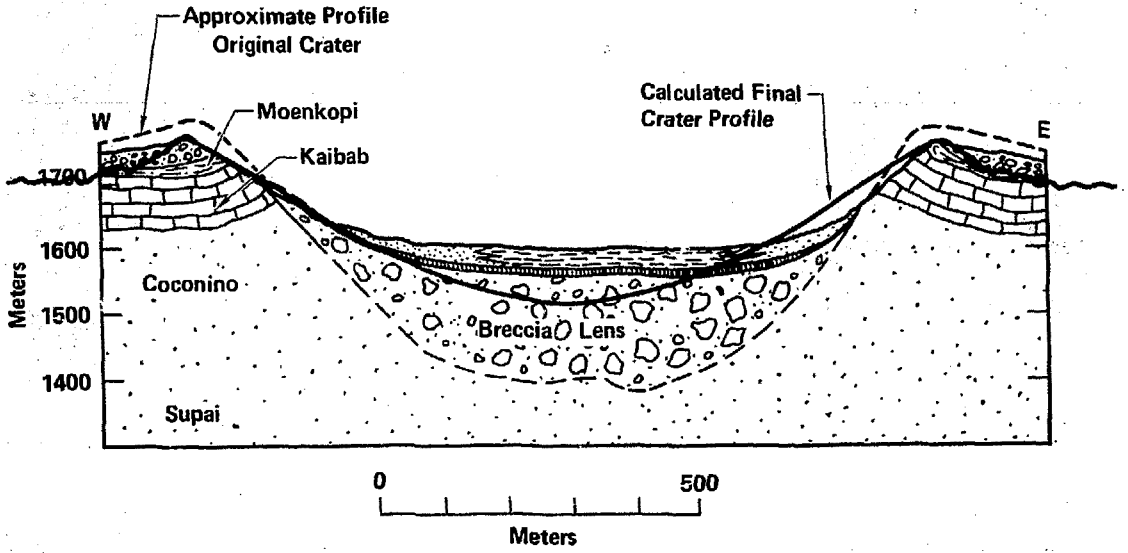

Bryan, J. B.
Crater Sim.
Figure 18

U.S. NUCLEAR CRATERS AND METEOR CRATER ARIZONA

Scaled apparent crater radius vs. scaled depth-of-burst

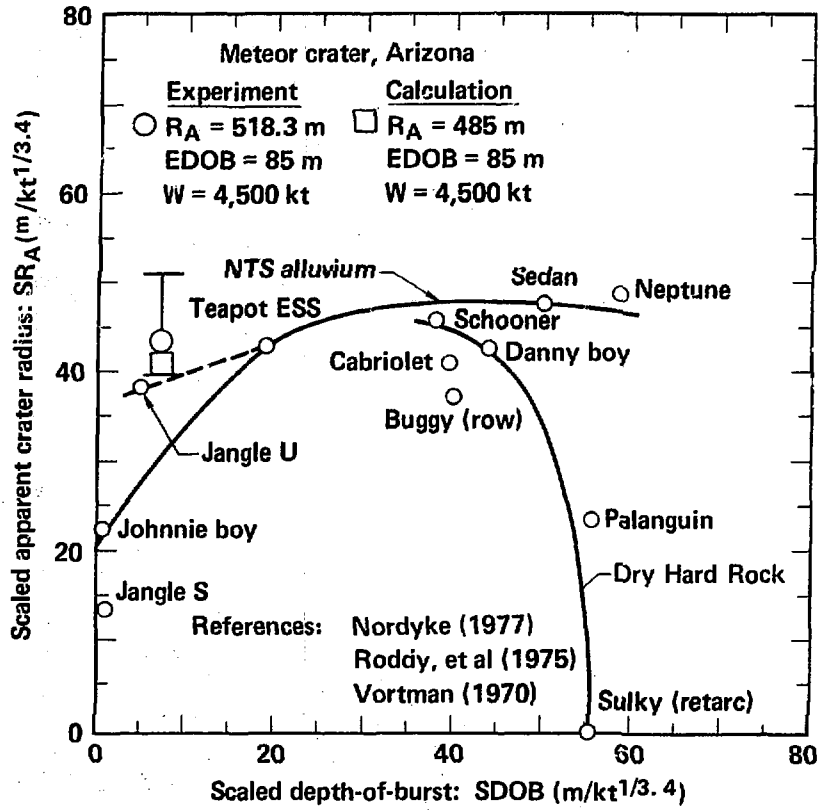

A kinetic energy value of 4,500 ± 1,800 kt was obtained for the meteorite using data from seven nuclear craters.

Bryan, J. B.
Crater. Sim.
Figure 19

U.S. NUCLEAR CRATERS AND METEOR CRATER, ARIZONA

Scaled apparent crater depth vs. scaled depth-of-burst

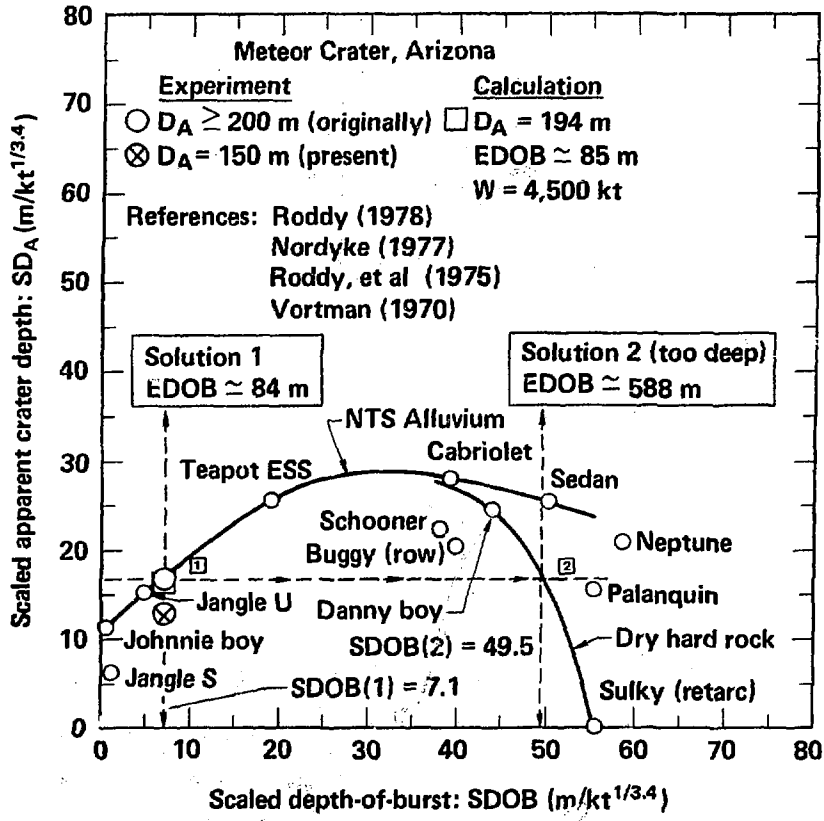

An effective depth-of-burst (EDOB) of about 84 m (vs. EDOB ≃ 85 m in the calculation) was obtained for the meteorite from the nuclear cratering curves.

Bryan, J. B.
Crater. Sim.
Figure 20